JACS
JOURNAL OF THE AMERICAN CHEMICAL SOCIETY

Article

pubs.acs.org/JACS

Tuning Cellular Uptake of Molecular Probes by Rational Design of Their Assembly into Supramolecular Nanoprobes

Lye Lin Lock,[†] Claudia D. Reyes,[†] Pengcheng Zhang,[†] and Honggang Cui*[,†,‡,§]

[†]Department of Chemical and Biomolecular Engineering, and Institute for NanoBioTechnology, The Johns Hopkins University, 3400 North Charles Street, Baltimore, Maryland 21218, United States

[‡]Department of Oncology and Sidney Kimmel Comprehensive Cancer Center, Johns Hopkins University School of Medicine, Baltimore, Maryland 21205, United States

[§]Center for Nanomedicine, The Wilmer Eye Institute, Johns Hopkins University School of Medicine, 400 North Broadway, Baltimore, Maryland 21231, United States

Supporting Information

ABSTRACT: Intracellular sensing of pathologically relevant biomolecules could provide essential information for accurate evaluation of disease staging and progression, yet the poor cellular uptake of water-soluble molecular probes limits their use as protease sensors. In other cases such as extracellular sensing, cellular uptake should be effectively inhibited. Self-assembly of molecular probes into supramolecular nanoprobes presents a potential strategy to alter their interaction mechanisms with cells to promote or reduce their cellular uptake. Here, we report on the design, synthesis, and assembly of peptide-based molecular beacons into supramolecular protease sensors of either spherical or filamentous shapes. We found that positively charged spherical nanobeacons demonstrate much higher cellular uptake efficiency than its monomeric form, thus making them most suitable for intracellular sensing of the lysosomal protease cathepsin B. Our results also suggest that assembly into filamentous nanobeacons significantly reduces their internalization by cancer cells, an important property that can be utilized for probing extracellular protease activities. These studies provide important guiding principles for rational design of supramolecular nanoprobes with tunable cellular uptake characteristics.

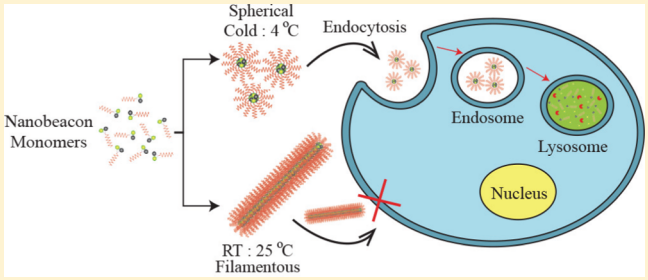

INTRODUCTION

The basis of optical imaging is to measure and process photonic signals generated as a result of specific interactions or reactions between the target biomolecules and rationally designed molecular probes.[1−3] As the reporting agent, molecular probes play a key role in translating biological information such as enzymatic activities or receptor locations into detectable signals. To obtain accurate diagnostic, therapeutic, or pathological information, molecular probes are often designed to have several important features including preference to accumulate in the targeted sites, specificity to bind/react with the molecular targets, ability to precisely translate the biological events into detectable signals, dispersion in aqueous media, and resistance to premature degradation during transportation. Because a large body of their molecular targets are located within cells, one particular challenge in utilizing water-soluble molecular probes for intracellular sensing is their effective uptake into cells of interest. Incorporating into the molecular design an auxiliary segment such as cell-penetrating peptides,[4] targeting ligands,[5] or linear hydrocarbons[6,7] is a widely explored strategy in the drug delivery community to enhance interactions of the resultant conjugates with cell membranes, thus leading to improved cellular uptake. However, because these conjugates still retain great water solubility, their risks of being prematurely degraded by nonspecific enzymes during transport have not been reduced. Recently, the work from the Mirkin lab has shown that high-density display of oligonucleotides on the surfaces of gold nanoparticles could improve both cellular uptake and resistance to enzymatic degradation.[8,9] We have also demonstrated that self-assembly of anticancer drugs into supramolecular nanostructures provides an effective means to improve their resistance to hydrolysis and enzymatic degradation.[10,11] On the basis of these findings, we reason that assembling molecular probes into supramolecular nanoprobes with tunable physicochemical characteristics would present an effective strategy to modulate their cellular uptake properties while improving their resistance to nonspecific degradation.

Many studies in the literature have shown that particle characteristics such as size, shape, and surface charge could affect to a great extent both their internalization efficiency and their endocytic pathways.[12−21] For example, the Chan lab investigated the intracellular uptake of different sized and

Received: January 8, 2016
Published: February 18, 2016

DOI: 10.1021/jacs.6b00073
J. Am. Chem. Soc. 2016, 138, 3533−3540

shaped colloidal gold nanoparticles and showed that the kinetics and saturation concentrations are highly dependent upon the physical dimensions of the nanoparticles.[14] The Chan lab also demonstrated that the receptor-mediated internalization can be regulated by using inorganic nanoparticles coated with antibodies, and their results suggested that nanoparticle size is a critical factor to determine the binding and activation of membrane receptors.[17] Mitragotri and co-workers reported that the internalization of micrometer-sized polystyrene particles by alveolar macrophages is primarily determined by the local shape of the particles, not by their size.[18,22,23] They proposed that the local particle shape plays a dominant role in initiating the phagocytosis process through interactions with cytoskeletons. Discher and co-workers studied the shape effect of filamentous nanostructures versus spherical objects in both in vivo and in vitro settings, and found that block copolymer filomicelles coated with a dense layer of polyethylene glycol (PEG) could circulate 10 times longer than their spherical counterparts in rodents.[15] Their in vitro experiments demonstrated that vesicles coated with PEG can be taken up more easily by activated macrophages, and that the phagocytosis efficiency of filomicelles strongly depends on their lengths, with the shorter ones being internalized at faster rates and filomicelles longer than 3 μm being hardly internalized. The DeSimone lab utilized a PRINT nanoparticle fabrication technique to generate monodisperse hydrogel particles ranging from 100 nm to 5 μm, and systematically studied their internalization by HeLa cells as a function of size, shape, and surface charge.[16] They concluded that rod-like particles of higher-aspect ratios are internalized more rapidly and more efficiently than the more symmetric ones. These pioneering studies suggest a complex interplay of cell types (phagocytic or nonphagocytic) with the particle characteristics and materials properties, but at the same time suggest the possibilities of modulating the cellular internalization of molecular probes by tuning the physicochemical properties of their assemblies.

Molecular beacons are activatable molecular probes typically containing a pair of fluorophores that were originally designed for sequence detections of DNA or RNA on the basis of a change in quenching status after binding with the target molecules.[24] This Förster resonance energy transfer (FRET)-based probe design is particularly useful in situations where probe-bound target molecules cannot be easily separated from unbound probes and other nontarget molecules. There has been a growing interest in the design of peptide-based molecular beacons to detect enzymatic activities of disease-relevant proteases.[25−29] We recently reported a rational design of supramolecular spherical nanobeacons that can be used to probe a cancer-relevant enzyme, cathepsin B (CatB).[11] Our previous results have shown that the assembled beacon is resistant to enzymatic degradation but upon dilution could dissociate into the monomeric form for effective cleavage by the target enzyme. Inspired by the tunable cellular uptake features of nanoparticles through changes in size, shape, and charge status, herein we designed and synthesized two self-assembling molecular beacons of exactly the same chemical structures except for their terminal residues: one with three positively charged lysines (K), the other with three negatively charged glutamic acids (E). Both molecules can be directed to assemble into either spherical or filamentous nanobeacons through the manipulation of their assembly kinetics. Using this unique system, we studied the interdependent relationship of the nanoparticle's shape and charge in regulating the cellular internalization of molecular beacons. These findings demonstrate the importance of a nanoparticle's shape in regulating cellular uptake, and also highlight the structural benefit of supramolecular nanobeacons over its monomeric form.

RESULTS AND DISCUSSION

Molecular Design. The key feature of our molecular design is to construct an amphiphilic nanobeacon with the central assembly regulating sequence, GNNQQNY heptapeptide, to promote the self-assembly of nanobeacons into different morphologies. The heptapeptide sequence is derived from $Sup35_{7-13}$, known to have a high propensity to form intermolecular hydrogen-bonded β-sheets.[30,31] To achieve the desired molecular characteristics for self-assembly, a hydrophobic quencher (Black Hole Quencher-1, BHQ-1) and a corresponding fluorophore 5-carboxyfluorescein (5-FAM) were covalently linked to the $Sup35_{7-13}$ with customizable hydrophilic charged ends, creating an amphiphilic molecular beacon (Figure 1). This peptide conjugation concept offers a versatile design platform for accessing a great diversity of nanostructures,[32] and has been used to construct peptide amphiphiles,[33−41] drug amphiphiles,[10] and other peptide-based self-assembling amphiphilic molecules.[42−44] Three lysines (K) or glutamic acids (E) were placed on the *C*-terminus of the $Sup35_{7-13}$ to obtain the positively charged **SFB-K** or negatively

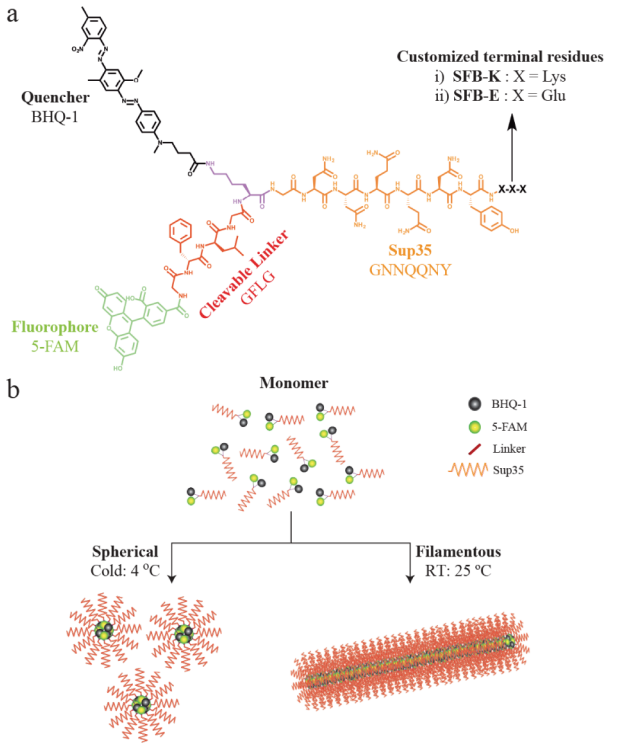

Figure 1. (a) Molecular design of the two studied self-assembling **SFB-K** and **SFB-E** molecular beacons, each containing four key design elements: (i) the Black Hole Quencher-1 (BHQ-1), (ii) the reporting agent 5-FAM, (iii) the central assembly regulating sequence GNNQQNY terminated with either three lysines (K) or glutamic acids (E), and (iv) the substrate -GFLG- with degradation specificity to a disease relevant protease, cathepsin B (CatB). (b) Both **SFB** molecular beacons are able to assemble into spherical or filamentous supramolecular nanobeacons, depending on both the assembly temperature and the incubation time.

DOI: 10.1021/jacs.6b00073
J. Am. Chem. Soc. 2016, 138, 3533−3540

charged **SFB-E** molecular beacons. Excluding the difference in terminal residues, the two studied molecules have identical chemical components. A tetrapeptide -GFLG- linker with known degradation specificity to the lysosomal enzyme cathepsin B (CatB) was used to connect the 5-FAM dye to the BHQ-1 quencher through a lysine junction.[45] CatB is a potential cancer marker for tumor screening, and has been reported to be related to tumor growth and progression.[46,47] The specific degradation of -GFLG- linker by CatB is expected to release 5-FAM from BHQ-1 quenching and resumes its fluorescence capacity, generating measurable optical signal for tracing the CatB locations. With this unique activatable feature, **SFB** fluorescence is detectable only upon cellular internalization and CatB activation, reducing the false-positive signal that could otherwise arise from nonspecific binding to the cell membrane. Both the **SFB-K** and the **SFB-E** molecular beacons were synthesized using a combination of automated and manual Fmoc solid-phase peptide synthesis (SPPS) methods as reported previously.[11] After RP-HPLC purification, the purity and expected molecular masses of the synthesized compounds were confirmed using analytical HPLC and mass spectrometry. Details for molecular synthesis and characterization are available in the Supporting Information, section S1.

Molecular Self-Assembly and Characterization. It has now been well recognized that the assembled morphology of the molecular building units can be influenced by both the experimental conditions and the kinetics pathways.[48−53] In the context of peptide assembly into filamentous nanostructures, Tirrell and co-workers have demonstrated the existence of spherical micelles as a transient morphology that would grow into filamentous micelles with increased incubation time at elevated temperature.[54] In our effort to obtain spherical and filamentous nanostructures, **SFB-K** and **SFB-E** molecules were both pretreated in hexafluoroisopropanol (HFIP) to eliminate any pre-existing aggregates that could potentially form during the peptide synthesis and purification processes. HFIP is a fluorinated alcohol commonly used to solubilize amyloid-forming peptides.[55] All HFIP treated samples were vacuum-dried using a rotary evaporator, followed by subsequent addition of a buffered solution to promote the formation of discrete nanostructures. After a certain period of incubation time, both cryogenic and staining-and-drying transmission electron microscopy (TEM) were utilized to characterize the morphology and dimensions of the assembled nanostructures.

We found that reconstitution of both **SFB-K** and **SFB-E** in 25 mM HEPES buffer to reach a final concentration of 200 μM led to the formation of spherical nanobeacons after aging the solutions for 1 day at 4 °C (Figure 2). TEM micrographs (Figure 2a,b) reveal dominant spherical nanostructures of a diameter of 7.8 ± 0.9 nm for **SFB-K** and a diameter of 7.6 ± 1.3 nm for **SFB-E**. Given the fully extended length of the **SFB** molecule (~5 nm) and the amphiphilic nature of the design, it is likely that assemblies have a core−shell structure. When the incubation temperature was increased to 25 °C, filamentous nanostructures became dominant for **SFB-K** after 3 days of aging. However, for **SFB-E**, the transformation of spherical to filamentous assemblies underwent a much slower process, only showing a mixture of spherical and filamentous nanostructures under the same experimental conditions. To achieve predominant filamentous structures for the latter in vitro cell studies, we directly dissolved lyophilized **SFB-E** powder in 1×DPBS buffer without HFIP pretreatment, followed by aging at 25 °C for 3 days. Our rationale was that the trace amount of preassembled structures during the peptide purification and lyophilization process could template the growth of the filamentous nanostructures. Indeed, **SFB-E** samples treated this way were found to form dominant filamentous morphology. TEM imaging (Figure 2c−d) revealed filamentous nanostructures of a diameter of 9.2 ± 1.9 and 8.9 ± 1.4 nm for **SFB-K** and **SFB-E**, respectively. The length of these filaments is in the range of tens of micrometers, which was estimated from TEM images taken at lower magnifications (Figure S4). Cryo-TEM was used to confirm that the observed filamentous assemblies were indeed formed in solution, not a result of drying during TEM sample preparation (Figure S5).

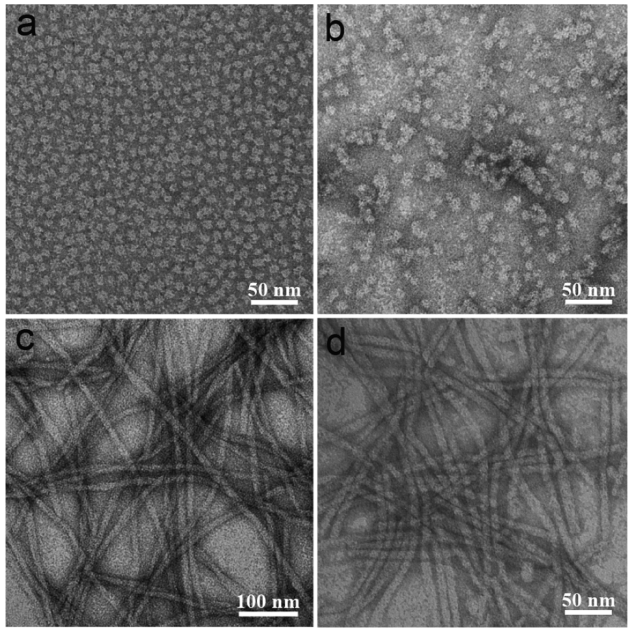

Figure 2. TEM micrographs of spherical and filamentous nanostructures formed by self-assembly of **SFB-K** (a,c) and **SFB-E** (b,d). All samples were prepared from the HFIP treated molecular beacons and reconstituted in 25 mM HEPES buffer to reach a final concentration of 200 μM, except filamentous **SFB-E** that was prepared by directly dissolving lyophilized **SFB-E** in 1×DPBS solution. All spherical nanostructures were kept at 4 °C for 1 day, while filamentous nanostructures were aged for at least 3 days at room temperature (25 °C).

The slightly larger diameters of the filaments than those of their respective spherical assemblies could stem from the variation in the peptide secondary structure affecting the degree of molecular stretching and packing. Circular dichroism (CD) measurements showed that both **SFB-K** and **SFB-E** adopted the random-coil conformation in their spherical assemblies, but exhibited typical β-sheet secondary structure absorption in filamentous assemblies (Figure S6). This observation is consistent with other studies in the literature where spherical and filamentous nanostructures assume different secondary structures.[56] These results also suggest that the emergence of the β-sheet conformation is important to promote the formation of the elongated (filamentous) structures.[38,56,57]

Zeta potential measurements were carried out to characterize the surface charge of these assembled nanostructures. As expected, spherical and filamentous **SFB-K** nanostructures containing the ε-amino group (primary amine) have a positive zeta potential of +40.7 ± 2.1 and +42.9 ± 0.7 mV, respectively, while the zeta potentials for spherical and filamentous **SFB-E**

DOI: 10.1021/jacs.6b00073
J. Am. Chem. Soc. 2016, 138, 3533−3540

assemblies were −50.2 ± 1.6 and −61.1 ± 6.2 mV, respectively. The negative surface charge of **SFB-E** nanostructures was attributed to the deprotonated γ-carboxyl and free *C*-terminus groups. The zeta potential measurement in our study is based on the electrophoretic mobility of particles in an applied electric field. In general, for spherical particles, the zeta potential measured by this method is independent upon the size. For charged long cylinders, however, their electrophoretic mobility depends on the particle's orientation relative to the applied electric field.[58−60] Upon transition from spherical micelles to filamentous nanobeacons, it is likely the solution viscosity will increase, so as to impact the measured electrophoretic mobility and consequently the zeta potential values. Therefore, given the complexity of comparing the zeta potentials between spherical and filamentous nanostructures, a definitive answer to explain the slightly increased zeta potential values from spheres to filaments is still lacking. Nevertheless, the measured zeta potential values suggest that the assembled nanostructures are stable in aqueous solutions.

Cellular Uptake. We investigated the effect of the surface charge, the nanostructure morphology, and the molecular assembly state (assembled versus unassembled/monomeric) on the cellular uptake of nanobeacons by cancer cells. As discussed earlier, the physicochemical properties of nanostructures could have a significant impact on their internalization pathways as a result of different interaction mechanisms with cell membranes.[8,61−64] To prepare unassembled molecular beacons, **SFB-K** and **SFB-E** were dissolved in dimethyl sulfoxide (DMSO), a solvent that can retain amyloid-β peptide in its monomeric state and is known to have minimal impact on the cell growth at low concentrations.[65] It is highly possible that upon adding the unassembled molecules into the cell media, some assembly could take place to form dimers, trimers, or even spherical assemblies. Although it is not clear to what extent the assembly could impact their cellular uptake, our cell studies suggest that this level of assembly is negligible within the time scale of cellular uptake experiments.

The cellular uptake of **SFB** nanobeacons was studied using PC3-Flu, a metastatic human prostate cancer cell line that has been reported to have overexpressed CatB activities associated with its aggressiveness.[66] The preseeded cells were treated with cell media containing 5 μM of **SFB** nanobeacons of respective shape, charge, and assembly state for 1 h. After removal of the beacon-containing cell medium, PC3-Flu cells were treated with 200 μL of Trypsin Gibco 0.25% Trypsin-EDTA (1×), phenol red, followed by a series of resuspension and centrifugation procedures. Flow cytometry was then used to quantify the released 5-FAM fluorescence within cells (Figure 3). Because only internalized **SFB** beacons can be activated by the lysosomal enzyme CatB and the activation rate of different molecular beacons regardless of surface charges, morphology, and molecular state fell into a comparable region (Figure S7), the geometric mean intensity of the released 5-FAM fluorescence can be used to compare the cellular uptake efficiency of the studied **SFB** beacons (Figure 3b,c,e,f). Figure 3a and d reveals the relative 5-FAM fluorescence intensity for all of the studied **SFB** beacons, by choosing the 5-FAM intensity of **SFB-K** spherical nanobeacon as a reference point.

The flow cytometry results revealed a significant difference in the cellular uptake of cationic spherical nanobeacon from its filamentous counterparts and monomeric forms (Figure 3a). PC3-Flu cells treated with cationic **SFB-K** spherical nanobeacons showed a ∼7-fold higher fluorescence than filamentous

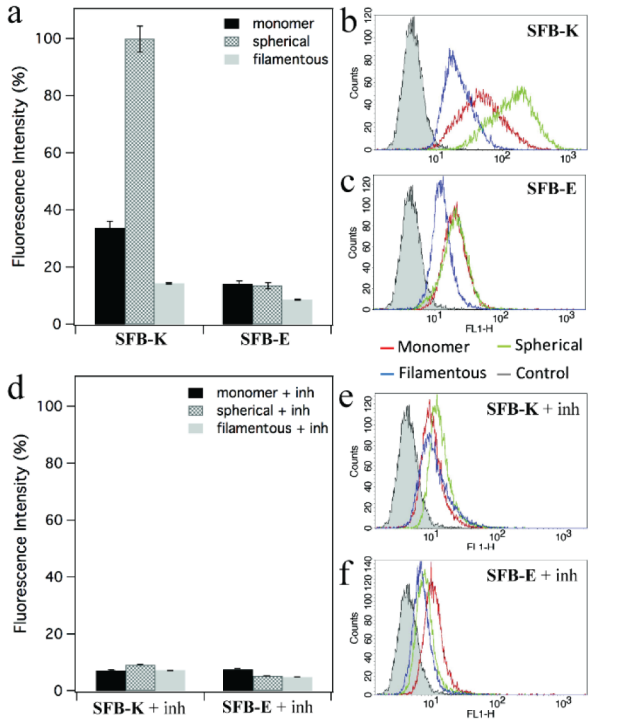

Figure 3. Effect of charge, shape, and assembly state of **SFB** beacons on the cellular uptake efficiency by cancer cells, characterized using flow cytometry. (a) Fluorescence intensity measurement suggests that spherical **SFB-K** nanobeacons were internalized faster than **SFB-K** monomeric beacon, and filamentous nanobeacons. Flow cytometry spectra comparing fluorescence intensity of different shapes of **SFB-K** (b) and **SFB-E**(c). (d) Upon inhibition of energy-dependent endocytosis pathway (+inh), PC3-Flu cells did not show appreciable uptake of **SFB** nanobeacons. Flow cytometry spectra comparing fluorescence intensity of different shapes of **SFB-K** (e) and **SFB-E** (f) in the presence of inhibitors for ATP production.

nanobeacons (14%). More importantly, the self-assembled form of **SFB-K** spherical nanobeacons showed ∼3-fold fluorescence increases as compared to the monomeric beacon (33%), presumably due to the enhanced interactions with cell membranes as a result of high charge density displayed on the nanobeacon surface.[8] Cellular uptake of nano-objects was known to be heavily impacted by the surface chemistry, with the cationic nanoparticles showing higher intracellular accumulation.[67] Similarly to our studies, cationic **SFB-K** nanobeacons were internalized faster than negatively charged **SFB-E** (Figure 3a). This phenomenon is most likely caused by the electrostatic interaction of cationic nanoparticles with a slightly anionic cell membrane.[67]

We also found that only the cellular uptake of spherical nanoparticles is greatly affected by their surface charge: cationic spherical nanoparticles fluoresced in cells ∼7 times higher than anionic spheres (14%). It is equally important to note that filamentous nanobeacons can hardly be internalized regardless of their charge status, and even showed reduced cellular uptake in comparison to monomeric beacon molecules. Figure 3a shows an approximately 2-fold decrease in 5-FAM fluorescence between filamentous nanobeacons (8−14%) and monomeric beacon (14−33%). We speculate that the elongated filaments spanning up to tens of micrometers in length were too big for the cells to engulf, consistent with the observation made by the Tirrell lab.[6] The high-aspect ratio of filamentous nanostructure

DOI: 10.1021/jacs.6b00073
J. Am. Chem. Soc. 2016, 138, 3533−3540

would require a much higher membrane bending energy, which is unfavorable for the cellular membrane wrapping process.[68]

We also performed TEM experiments to verify the stability of spherical and filamentous nanostructures under the condition of the cellular uptake experiments. Figure S8 shows the TEM micrographs collected from 5 μM **SFB** solutions after 1 h incubation at 37 °C, suggesting that **SFB** spherical and filamentous nanostructures were able to maintain their morphology in physiological buffers and cell media. We therefore conclude that the observed differences in cellular uptake of various nanobeacons arose from their distinction in the assembled state.

To better understand the greater intracellular accumulation of cationic spherical nanobeacons, we investigated the potential mode of their cellular entry. It has been shown that nanoparticles could enter cells via energy-dependent endocytosis or translocate through the cell membrane via a passive mechanism, depending on their shape and surface charge.[69−72] In our studies, we utilized a combination of sodium azide (NaN_3) and 2-deoxy-D-glucose (DDG)[73] to inhibit the metabolic activity of cells. NaN_3 inhibits ATPase activity to reduce cellular ATP production capability, while DDG depletes intracellular ATP storage.[74,75] PC3-Flu cells were first preincubated with 10 mM NaN_3 and 10 mM DDG for 15 min, and then were incubated with 5 μM **SFB** nanobeacons for 1 h at 37 °C. Presumably, these inhibitors would limit the energy-dependent endocytosis due to the lack of intracellular ATP. To demonstrate that PC3-Flu cells remained viable under the treatment of inhibitors, a cell cytotoxicity assay was performed with various concentrations of inhibitors that confirmed the viability of cells (Figure S11). The inhibition result in Figure 3d showed that the cellular uptake of all **SFB** nanobeacons was reduced to basal level (<10%), clearly indicating the cellular uptake of these conjugates follows the energy-dependent endocytosis pathway in all studied cases.

Cell Imaging. To verify that **SFB** nanobeacons were indeed internalized to generate intracellular 5-FAM fluorescence upon enzymatic activation, nanobeacon-treated live cell imaging was conducted using confocal microscopy. PC3-Flu cell nuclei were stained blue using Hoechst 33342, and the released 5-FAM from **SFB** nanobeacons by CatB protease cleavage would emit the green fluorescence. The confocal images (Figure 4) revealed clearly that the strongest fluorescence came from the cells treated with positively charged **SFB-K** spherical nanobeacon (Figure 4b), followed by the **SFB-K** monomeric beacon (Figure 4a). On the other hand, the 5-FAM green fluorescence can be barely seen for all of the negatively charged and filamentous nanobeacons (Figure 4c−f), suggesting marginal cellular uptake in these studies. This observation is consistent with the fluorescence intensity trend quantified by flow cytometry analysis in Figure 3a. Because it has been widely reported that the positively charged particles can induce temporary transmembrane pores that can cause potential toxicity to the cells,[76−78] we evaluated the cell viability of PC3-Flu cell treated with nanobeacons of different shapes and surface charges. The result in Figure S10 showed that cell viability remained high (>95%) under these experimental conditions.

To further examine the intracellular distribution of the spherical **SFB-K** nanobeacons, PC3-Flu cells were treated with Lysotracker Red to label the lysosomal compartments in the cells. The merged image of 5-FAM green fluorescence (Figure 5a) and lysotracker red (Figure 5b), shown in yellow (Figure 5c), indicated the colocalization of 5-FAM with the lysosome. In addition, the spatial-intensity profile analysis of PC3-Flu cells (inset: white line along PC3-Flu cells) in Figure 5d,e signifies the overlap of 5-FAM green and lysotracker red fluorescence. The fluorescence intensities of 5-FAM and lysotracker red were quantified, and the weighted colocalization coefficient was determined to be 86.5 ± 8.4% (n = 20 cells) using ZEN image processing software, which supports the high correlation of 5-FAM with the lysosomal compartments. Because lysosomes are often associated with the late stages of endocytic pathways, this finding further validates that spherical **SFB-K** nanobeacons were internalized through endocytosis. This also suggests that, if cytosolic accumulation or other organelle-specific deposition is required, an endosomal escape mechanism should be incorporated into the nanobeacon design to facilitate intracellular trafficking to its target sites.

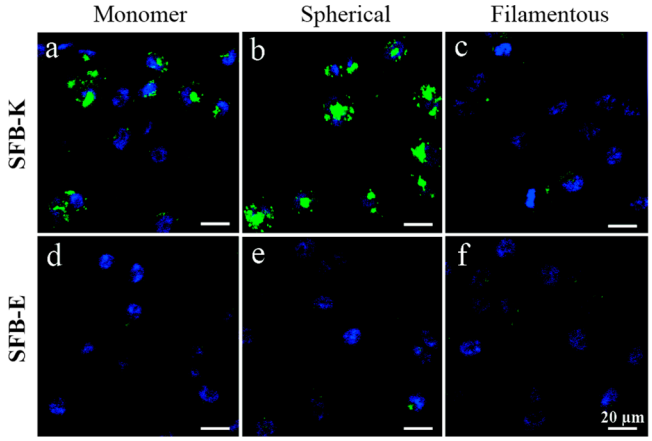

Figure 4. Confocal laser scanning microscopy of PC3-Flu cells after 1 h of incubation with 5 μM of **SFB** nanobeacons in different shapes and surface charges. Beacon monomers, spherical, and filamentous assemblies of (a−c) **SFB-K** and (d−f) **SFB-E**, respectively. All scale bars: 20 μm.

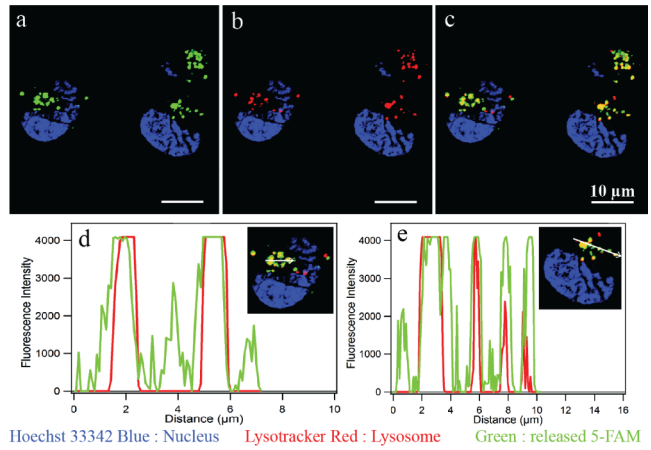

Figure 5. Confocal microscopy images of (a) released 5-FAM (green) and (b) Lysotracker Red staining lysosome (red) of PC3-Flu cells after incubation with 5 μM of spherical **SFB-K** for 1 h. (c) Overlay of green and red channels showed colocalization of released 5-FAM in lysosome. (d,e) Spatial-intensity profile of PC3-Flu cell along the white line imposed on the inset images. Colocalization of green and red channels was quantified, and the weighted colocalization coefficient was determined to be 86.5 ± 8.4% (n = 20 cells).

DOI: 10.1021/jacs.6b00073
J. Am. Chem. Soc. 2016, 138, 3533−3540

CONCLUSION

In this study, we demonstrated the design and construction of both spherical and filamentous supramolecular imaging probes, and investigated the effect of their shape, charge, and assembled state on the internalization by cancer cells. Our findings shed light on the development of supramolecular imaging agents for cancer therapeutics and diagnostics from two significant perspectives. First, our results demonstrated the possibilities of constructing supramolecular imaging agents of various morphologies through rational design of the chemical structures of the imaging agent. The advancement in conjugation chemistry and peptide chemistry allows for covalent linkage of almost any functional units with rationally designed auxiliary units to create new conjugates capable of assembling into a variety of nanostructures in aqueous conditions. For these supramolecular probes, it is the physicochemical properties of the assembled nanostructures rather than the molecular characteristics of the building units that determine the eventual circulation fate and cell interaction outcomes. Although not demonstrated in this Article, it is well expected these supramolecular beacons could improve the imaging sensitivity and specificity by delivering a cluster of molecular probes to the target disease sites. We believe that this supramolecular strategy opens a new avenue in molecular imaging that could benefit many areas of biomedical research. Second, our results suggest formation of supramolecular nanostructures could improve or reduce their internalization by cancer cells. Cationic spherical nanobeacons (**SFB-K**) outperform monomeric beacon and filamentous nanobeacons, demonstrating the highest cellular uptake efficiency. This clearly suggests that for intracellular sensing, spherical objects of positive charges would be the most logical design. In sharp contrast, assembly of molecular beacons into filamentous nanobeacons regardless of charge status significantly reduces its cellular uptake efficiency and did not show any noticeable internalization under our experimental conditions. Therefore, these filamentous nanobeacons could be used for sensing extracellular proteases such as matrix metalloproteases, for which internalization should be prevented. We hope that these promising results will motivate more researchers to work in the area of supramolecular imaging.

MATERIALS AND METHODS

Self-Assembly of Spherical and Filamentous Nanostructures. HFIP (hexafluoroisopropanol), known to break amyloid-β interactions into homogeneous monomeric form, was used in this sample preparation procedure. **SFB-K** and **SFB-E** molecules were first dissolved in HFIP, and the concentration was calibrated to 200 μM in 200 μL of HFIP. HFIP was then removed using a rotary evaporator in a 40 °C water bath for 10 min, leaving a thin film of dried nanobeacons on the wall of the glass vial.

For the monomer preparation, all samples were reconstituted in 200 μL of DMSO, yielding a final concentration of 200 μM, and were kept at room temperature. For the spherical nanostructure formation, all samples were first reconstituted in 50 μL of 100 mM HEPES buffer, 150 μL of water was subsequently added to yield a final sample concentration of 200 μM in 200 μL of 25 mM of HEPES buffer, and all samples were kept at 4 °C. In the preparation of filamentous nanostructures, **SFB-K** was first dissolved in 50 μL of 100 mM HEPES buffer, and 150 μL of water was subsequently added to yield a final sample concentration of 200 μM in 200 μL of 25 mM of HEPES buffer. These samples were sonicated in a water bath for 20 min and kept at room temperature. For filamentous **SFB-E** nanobeacons, **SFB-E** lyophilized powder was dissolved directly in 1×DPBS solution to yield a final concentration of 200 μM and was stored at room temperature.

Transmission Electron Microscopy (TEM) and Cryo-TEM. Five microliters of each sample was spotted on a carbon film copper grid with 400 square mesh (from EMS: Electron Microscopy Sciences), and the excess was removed using filter paper to leave a thin film of sample on the grid. After letting the sample dry for 10 min, 5 μL of 2% uranyl acetate was added to sample grid, and the excess was removed after 10 s. All samples were dried for at least 2 h before TEM imaging.

Cryogenic TEM imaging was also performed on the FEI Tecnai 12 TWIN transmission electron microscope, operating at 80 kV. 3−5 μL of sample solution was placed on a lacey carbon film supported on a TEM copper grid (Electron Microscopy Services, Hatfield, PA). All of the TEM grids used for cryo-TEM imaging were treated with plasma air to render the lacey carbon film hydrophilic. A thin film of the sample solution was produced using the Vitrobot with a controlled humidity chamber (FEI). After loading of the sample solution, the lacey carbon grid was blotted using preset parameters and plunged instantly into a liquid ethane reservoir precooled by liquid nitrogen. The vitrified samples were then transferred to a cryo-holder and cryo-transfer stage, which was cooled by liquid nitrogen. To prevent sublimation of vitreous water, the cryo-holder temperature was maintained below −170 °C during the imaging process. All images were recorded by a SIS Megaview III wide-angle CCD camera.

Zeta Potential Measurement. Zeta potential measurements were carried out using a Malvern Zetasizer Nano instrument and its compatible disposable capillary cell (DTS 1070 from Malvern). Spherical and filamentous **SFB** nanobeacons were instantly diluted from 200 to 5 μM in water with a final volume of 1 mL. Measurements were carried out in automated mode and repeated three times to obtain an average value and its standard deviation.

Activation of Nanobeacon with Cathepsin B Enzyme. CatB enzymatic reaction buffer was prepared in 50 mM sodium acetate buffer with 25 mM L-cystein as enzyme activator, and 1 mM EDTA was added as enzyme stabilizer. 0.025 unit of CatB was preincubated in reaction buffer for 5 min at 37 °C to activate the enzyme, and **SFB** nanobeacons were added to reaction buffer to yield a final concentration of 1 μM and a final volume of 100 μL. All samples were triplicated, and the experiment was carried out in a 96-well standard opaque plate. 5-FAM molecule was excited at 492 nm, and emission was collected at 520 nm with a 515 nm cut off. Using a Gemini XPS microplate reader (Molecular Devices, Sunnyvale, CA), the kinetic mode was selected and fluorescence intensity was measured at different time points.

In Vitro Cellular Uptake and Inhibition Studies Using Flow Cytometry. PC3-Flu cells were seeded onto a 24-well plate with cell density of 1×10^5 cells/well and incubated at 37 °C, in 5% CO_2 overnight. 5 μM **SFB** nanobeacons (monomers, spherical, and filamentous, independently) was prepared by adding 12.5 μL of 200 μM **SFB** stock solution into 487.5 μL of 1640 cell medium for PC3-Flu. PC3-Flu cells were incubated with the cell medium containing 5 μM of **SFB** nanobeacons for 1 h in 37 °C. On the other hand, the energy-dependent endocytosis was inhibited by pretreatment with 10 mM sodium azide and 10 mM 2-deoxy-D-glucose for 15 min, followed by 5 μM **SFB** nanobeacons incubation for 1 h in 37 °C. Cell medium was removed, and 200 μL of Trypsin Gibco 0.25% Trypsin-EDTA (1×), phenol red (Life Technologies Corporation) was added to PC3-Flu cells and incubated for 2 min at room temperature. 500 μL of 1640 cell medium was added to each well, and cells were resuspended from the bottom of each well, then transferred into a 1.5 mL Eppendoff tube and kept on ice. All cells were centrifuged at 1.7k RPM for 90 s, and the supernatant was removed. 500 μL of cold 1×DPBS was added to wash cells and recentrifuged at 1.7k RPM for 90 s. The supernatant was removed, and 200 μL of cold 1×DPBS was added to resuspend cells, and then transferred into a flow-cytometry tube. 10 000 live cells were gated, and fluorescence intensity was detected using a flow cytometer (FACSCalibur, BD).

Confocal Laser Scanning Microscopy. PC3-Flu was seeded onto an 8-well plate with a cell density of 3×10^4 cells/well and incubated overnight in a 37 °C incubator. 7.5 μL of 200 μM **SFB**

DOI: 10.1021/jacs.6b00073
J. Am. Chem. Soc. 2016, 138, 3533−3540

nanobeacons was added to 292.5 μL of 1640 cell medium and transferred to each well containing PC3-Flu cells. The cells were kept at 37 °C for 1 h and then the medium was removed, followed by a quick wash with 300 μL of cell medium without phenyl red. PC3-Flu cells were imaged directly without fixing the cells. The cell nuclei were stained in blue with Hoechst 33342, and lysosome compartments were stained with Lysotracker Red for 30 min before the cell imaging.

■ ASSOCIATED CONTENT

Supporting Information

The Supporting Information is available free of charge on the ACS Publications website at DOI: 10.1021/jacs.6b00073.

Details of molecular synthesis and characterization, procedure to control the shape of self-assembled nanobeacons, CD measurement, cathepsin B enzymatic activation, stability of nanostructures, and cytotoxicity evaluation (PDF)

■ AUTHOR INFORMATION

Corresponding Author

*hcui6@jhu.edu

Notes

The authors declare no competing financial interest.

■ ACKNOWLEDGMENTS

The work reported here is supported by the National Science Foundation (DMR 1255281), the National Institutes of Health (NIH/1R21CA191740), and W. W. Smith Charitable Trust. We thank the Integrated Imaging Center (IIC) at The Johns Hopkins University for TEM, cryo-TEM imaging, and confocal microscopy. We also thank Dr. Martin Pomper (Department of Radiology, JHMI) for providing the PC3-Flu cell line.

■ REFERENCES

(1) Weissleder, R. *Science* **2006**, *312*, 1168−1171.
(2) Willmann, J. K.; van Bruggen, L. M.; Dinkelborg, L. M.; Gambhir, S. S. *Nat. Rev. Drug Discovery* **2008**, *7*, 591−607.
(3) Chen, K.; Chen, X. Y. *Curr. Top. Med. Chem.* **2010**, *10*, 1227−1236.
(4) Wender, P. A.; Mitchell, D. J.; Pattabiraman, K.; Pelkey, E. T.; Steinman, L.; Rothbard, J. B. *Proc. Natl. Acad. Sci. U. S. A.* **2000**, *97*, 13003−13008.
(5) Banerjee, S. R.; Pullambhatla, M.; Foss, C. A.; Nimmagadda, S.; Ferdani, R.; Anderson, C. J.; Mease, R. C.; Pomper, M. G. *J. Med. Chem.* **2014**, *57*, 2657−2669.
(6) Missirlis, D.; Khant, H.; Tirrell, M. *Biochemistry* **2009**, *48*, 3304−3314.
(7) Zhang, P.; Lock, L. L.; Cheetham, A. G.; Cui, H. *Mol. Pharmaceutics* **2014**, *11*, 964−973.
(8) Choi, C. H. J.; Hao, L. L.; Narayan, S. P.; Auyeung, E.; Mirkin, C. A. *Proc. Natl. Acad. Sci. U. S. A.* **2013**, *110*, 7625−7630.
(9) Rosi, N. L.; Giljohann, D. A.; Thaxton, C. S.; Lytton-Jean, A. K. R.; Han, M. S.; Mirkin, C. A. *Science* **2006**, *312*, 1027−1030.
(10) Cheetham, A. G.; Zhang, P. C.; Lin, Y. A.; Lock, L. L.; Cui, H. G. *J. Am. Chem. Soc.* **2013**, *135*, 2907−2910.
(11) Lock, L. L.; Cheetham, A. G.; Zhang, P. C.; Cui, H. G. *ACS Nano* **2013**, *7*, 4924−4932.
(12) Agarwal, R.; Singh, V.; Jurney, P.; Shi, L.; Sreenivasan, S. V.; Roy, K. *Proc. Natl. Acad. Sci. U. S. A.* **2013**, *110*, 17247−17252.
(13) Albanese, A.; Walkey, C. D.; Olsen, J. B.; Guo, H.; Emili, A.; Chan, W. C. W. *ACS Nano* **2014**, *8*, 5515−5526.
(14) Chithrani, B. D.; Ghazani, A. A.; Chan, W. C. W. *Nano Lett.* **2006**, *6*, 662−668.
(15) Geng, Y.; Dalhaimer, P.; Cai, S. S.; Tsai, R.; Tewari, M.; Minko, T.; Discher, D. E. *Nat. Nanotechnol.* **2007**, *2*, 249−255.
(16) Gratton, S. E. A.; Ropp, P. A.; Pohlhaus, P. D.; Luft, J. C.; Madden, V. J.; Napier, M. E.; DeSimone, J. M. *Proc. Natl. Acad. Sci. U. S. A.* **2008**, *105*, 11613−11618.
(17) Jiang, W.; Kim, B. Y. S.; Rutka, J. T.; Chan, W. C. W. *Nat. Nanotechnol.* **2008**, *3*, 145−150.
(18) Kolhar, P.; Anselmo, A. C.; Gupta, V.; Pant, K.; Prabhakarpandian, B.; Ruoslahti, E.; Mitragotri, S. *Proc. Natl. Acad. Sci. U. S. A.* **2013**, *110*, 10753−10758.
(19) Rejman, J.; Oberle, V.; Zuhorn, I. S.; Hoekstra, D. *Biochem. J.* **2004**, *377*, 159−169.
(20) Tang, L.; Yang, X. J.; Yin, Q.; Cai, K. M.; Wang, H.; Chaudhury, I.; Yao, C.; Zhou, Q.; Kwon, M.; Hartman, J. A.; Dobrucki, I. T.; Dobrucki, L. W.; Borst, L. B.; Lezmig, S.; Helferich, W. G.; Ferguson, A. L.; Fan, T. M.; Cheng, J. J. *Proc. Natl. Acad. Sci. U. S. A.* **2014**, *111*, 15344−15349.
(21) Zhang, S. L.; Li, J.; Lykotrafitis, G.; Bao, G.; Suresh, S. *Adv. Mater.* **2009**, *21*, 419−424.
(22) Champion, J. A.; Katare, Y. K.; Mitragotri, S. *J. Controlled Release* **2007**, *121*, 3−9.
(23) Champion, J. A.; Mitragotri, S. *Proc. Natl. Acad. Sci. U. S. A.* **2006**, *103*, 4930−4934.
(24) Tyagi, S.; Kramer, F. R. *Nat. Biotechnol.* **1996**, *14*, 303−308.
(25) Chen, J.; Liu, T. W. B.; Lo, P. C.; Wilson, B. C.; Zheng, G. *Bioconjugate Chem.* **2009**, *20*, 1836−1842.
(26) Lee, S.; Xie, J.; Chen, X. Y. *Curr. Top. Med. Chem.* **2010**, *10*, 1135−1144.
(27) Olson, E. S.; Jiang, T.; Aguilera, T. A.; Nguyen, Q. T.; Ellies, L. G.; Scadeng, M.; Tsien, R. Y. *Proc. Natl. Acad. Sci. U. S. A.* **2010**, *107*, 4311−4316.
(28) Thurley, S.; Roglin, L.; Seitz, O. *J. Am. Chem. Soc.* **2007**, *129*, 12693−12695.
(29) Zheng, G.; Chen, J.; Stefflova, K.; Jarvi, M.; Li, H.; Wilson, B. C.; Thurley, S.; Roglin, L.; Seitz, O. *J. Am. Chem. Soc.* **2007**, *129*, 12693.
(30) Hamley, I. W. *Chem. Rev.* **2012**, *112*, 5147−5192.
(31) Nelson, R.; Sawaya, M. R.; Balbirnie, M.; Madsen, A. O.; Riekel, C.; Grothe, R.; Eisenberg, D. *Nature* **2005**, *435*, 773−778.
(32) Han, S. Y.; Cao, S. S.; Wang, Y. M.; Wang, J. Q.; Xia, D. H.; Xu, H.; Zhao, X. B.; Lu, J. R. *Chem. - Eur. J.* **2011**, *17*, 13095−13102.
(33) Cui, H. G.; Cheetham, A. G.; Pashuck, E. T.; Stupp, S. I. *J. Am. Chem. Soc.* **2014**, *136*, 12461−12468.
(34) Cui, H. G.; Webber, M. J.; Stupp, S. I. *Biopolymers* **2010**, *94*, 1−18.
(35) Hartgerink, J. D.; Beniash, E.; Stupp, S. I. *Science* **2001**, *294*, 1684−1688.
(36) Lowik, D. W. P. M.; Garcia-Hartjes, J.; Meijer, J. T.; van Hest, J. C. M. *Langmuir* **2005**, *21*, 524−526.
(37) Missirlis, D.; Chworos, A.; Fu, C. J.; Khant, H. A.; Krogstad, D. V.; Tirrell, M. *Langmuir* **2011**, *27*, 6163−6170.
(38) Paramonov, S. E.; Jun, H. W.; Hartgerink, J. D. *J. Am. Chem. Soc.* **2006**, *128*, 7291−7298.
(39) Pashuck, E. T.; Cui, H. G.; Stupp, S. I. *J. Am. Chem. Soc.* **2010**, *132*, 6041−6046.
(40) Stendahl, J. C.; Rao, M. S.; Guler, M. O.; Stupp, S. I. *Adv. Funct. Mater.* **2006**, *16*, 499−508.
(41) Stupp, S. I.; Zha, R. H.; Palmer, L. C.; Cui, H. G.; Bitton, R. *Faraday Discuss.* **2013**, *166*, 9−30.
(42) Bai, S.; Pappas, C.; Debnath, S.; Frederix, P. W. J. M.; Leckie, J.; Fleming, S.; Ulijn, R. V. *ACS Nano* **2014**, *8*, 7005−7013.
(43) Cavalli, S.; Albericio, F.; Kros, A. *Chem. Soc. Rev.* **2010**, *39*, 241−263.
(44) Kuang, Y.; Du, X. W.; Zhou, J.; Xu, B. *Adv. Healthcare Mater.* **2014**, *3*, 1217−1221.
(45) Duncan, R.; Cable, H. C.; Lloyd, J. B.; Rejmanova, P.; Kopecek, J. *Makromol. Chem.* **1983**, *184*, 1997−2008.
(46) Jedeszko, C.; Sloane, B. F. *Biol. Chem.* **2004**, *385*, 1017−1027.
(47) Weissleder, R.; Tung, C. H.; Mahmood, U.; Bogdanov, A., Jr. *Nat. Biotechnol.* **1999**, *17*, 375−378.
(48) Gosal, W. S.; Morten, I. J.; Hewitt, E. W.; Smith, D. A.; Thomson, N. H.; Radford, S. E. *J. Mol. Biol.* **2005**, *351*, 850−864.

DOI: 10.1021/jacs.6b00073
J. Am. Chem. Soc. 2016, 138, 3533−3540

(49) Jonkheijm, P.; van der Schoot, P.; Schenning, A. P. H. J.; Meijer, E. W. *Science* **2006**, *313*, 80−83.
(50) Korevaar, P. A.; Newcomb, C. J.; Meijer, E. W.; Stupp, S. I. *J. Am. Chem. Soc.* **2014**, *136*, 8540−8543.
(51) Pappas, C. G.; Sasselli, I. R.; Ulijn, R. V. *Angew. Chem., Int. Ed.* **2015**, *54*, 8119−8123.
(52) Tantakitti, F.; Boekhoven, J.; Wang, X.; Kazantsev, R. V.; Yu, T.; Li, J.; Zhuang, E.; Zandi, R.; Ortony, J. H.; Newcomb, C. J.; Palmer, L. C.; Shekhawat, G. S.; Olvera de la Cruz, M.; Schatz, G. C.; Stupp, S. I. *Nat. Mater.* **2016**, DOI: 10.1038/nmat4538.
(53) Zhang, Y.; Zhou, N.; Shi, J. F.; Pochapsky, S. S.; Pochapsky, T. C.; Zhang, B.; Zhang, X. X.; Xu, B. *Nat. Commun.* **2015**, *6*.
(54) Shimada, T.; Sakamoto, N.; Motokawa, R.; Koizumi, S.; Tirrell, M. *J. Phys. Chem. B* **2012**, *116*, 240−243.
(55) Stine, W. B.; Dahlgren, K. N.; Krafft, G. A.; LaDu, M. J. *J. Biol. Chem.* **2003**, *278*, 11612−11622.
(56) Shimada, T.; Lee, S.; Bates, F. S.; Hotta, A.; Tirrell, M. *J. Phys. Chem. B* **2009**, *113*, 13711−13714.
(57) Velichko, Y. S.; Stupp, S. I.; Olvera de la Cruz, M. *J. Phys. Chem. B* **2008**, *112*, 2326−2334.
(58) Ohshima, H. *Langmuir* **2015**, *31*, 13633−13638.
(59) Stigter, D. *J. Phys. Chem.* **1978**, *82*, 1417−1423.
(60) Stigter, D. *J. Phys. Chem.* **1978**, *82*, 1424−1429.
(61) Nel, A. E.; Madler, L.; Velegol, D.; Xia, T.; Hoek, E. M. V.; Somasundaran, P.; Klaessig, F.; Castranova, V.; Thompson, M. *Nat. Mater.* **2009**, *8*, 543−557.
(62) Yim, E. K.; Leong, K. W. *Nanomedicine* **2005**, *1*, 10−21.
(63) Zhang, K.; Fang, H. F.; Chen, Z. Y.; Taylor, J. S. A.; Wooley, K. L. *Bioconjugate Chem.* **2008**, *19*, 1880−1887.
(64) Zhang, K.; Rossin, R.; Hagooly, A.; Chen, Z. Y.; Welch, M. J.; Wooley, K. L. *J. Polym. Sci., Part A: Polym. Chem.* **2008**, *46*, 7578−7583.
(65) Shen, C. L.; Murphy, R. M. *Biophys. J.* **1995**, *69*, 640−651.
(66) Szpaderska, A. M.; Frankfater, A. *Cancer Res.* **2001**, *61*, 3493−3500.
(67) Chen, L.; McCrate, J. M.; Lee, J. C.; Li, H. *Nanotechnology* **2011**, *22*, 105708.
(68) Dasgupta, S.; Auth, T.; Gompper, G. *Nano Lett.* **2014**, *14*, 687−693.
(69) Beddoes, C. M.; Case, C. P.; Briscoe, W. H. *Adv. Colloid Interface Sci.* **2015**, *218*, 48−68.
(70) Lin, J. Q.; Alexander-Katz, A. *ACS Nano* **2013**, *7*, 10799−10808.
(71) Osaki, F.; Kanamori, T.; Sando, S.; Sera, T.; Aoyama, Y. *J. Am. Chem. Soc.* **2004**, *126*, 6520−6521.
(72) Wang, T. T.; Bai, J.; Jiang, X.; Nienhaus, G. U. *ACS Nano* **2012**, *6*, 1251−1259.
(73) Steinman, R. M.; Silver, J. M.; Cohn, Z. A. *J. Cell Biol.* **1974**, *63*, 949−969.
(74) Unno, N.; Menconi, M. J.; Salzman, A. L.; Smith, M.; Hagen, S.; Ge, Y. M.; Ezzell, R. M.; Fink, M. P. *Am. J. Physiol.-Gastr. L* **1996**, *270*, G1010−G1021.
(75) Vasilyeva, E.; Forgac, M. *J. Biol. Chem.* **1998**, *273*, 23823−23829.
(76) Chen, J. M.; Hessler, J. A.; Putchakayala, K.; Panama, B. K.; Khan, D. P.; Hong, S.; Mullen, D. G.; DiMaggio, S. C.; Som, A.; Tew, G. N.; Lopatin, A. N.; Baker, J. R.; Holl, M. M. B.; Orr, B. G. *J. Phys. Chem. B* **2009**, *113*, 11179−11185.
(77) Hong, S. P.; Leroueil, P. R.; Janus, E. K.; Peters, J. L.; Kober, M. M.; Islam, M. T.; Orr, B. G.; Baker, J. R.; Holl, M. M. B. *Bioconjugate Chem.* **2006**, *17*, 728−734.
(78) Sovadinova, I.; Palermo, E. F.; Huang, R.; Thoma, L. M.; Kuroda, K. *Biomacromolecules* **2011**, *12*, 260−268.

DOI: 10.1021/jacs.6b00073
J. Am. Chem. Soc. 2016, 138, 3533−3540